

# Contribution of Fluorine to Protein–Ligand Affinity in the Binding of Fluoroaromatic Inhibitors to Carbonic Anhydrase II

Chu-Young Kim,<sup>†</sup> Jeanne S. Chang,<sup>‡</sup> Jeffrey B. Doyon,<sup>‡</sup> Teaster T. Baird, Jr.,<sup>⊥</sup>  
Carol A. Fierke,<sup>||</sup> Ahamindra Jain,<sup>\*,‡,§</sup> and David W. Christianson<sup>\*,†</sup>

Contribution from Roy and Diana Vagelos Laboratories, Department of Chemistry, University of Pennsylvania, Philadelphia, Pennsylvania 19104-6323, Department of Chemistry, Swarthmore College, Swarthmore, Pennsylvania 19081-1397, Department of Pharmaceutical Chemistry, University of California, San Francisco, San Francisco, California 94143, Department of Chemistry, University of Michigan, Ann Arbor, Michigan 48109, and Department of Chemistry, University of California, Berkeley, Berkeley, California 94720-1460

Received July 17, 2000

**Abstract:** Carbonic anhydrase II (CAII) is a zinc metalloenzyme that catalyzes the hydration of CO<sub>2</sub> to yield bicarbonate and a proton. *N*-(4-Sulfamylbenzoyl)benzylamine (SBB) is a tight-binding inhibitor of human CAII with  $K_d = 2.1$  nM. Previous X-ray crystallographic work shows that the benzyl ring of SBB makes an edge-to-face interaction with Phe-131 in the enzyme active site. We have manipulated the electrostatics of this interaction by systematically substituting electronegative fluorine atoms for the benzyl ring hydrogens of SBB. Crystal structures of 10 enzyme–inhibitor complexes have been determined to atomic resolution. Analysis of these structures reveals that the main contributions to enzyme–inhibitor affinity can be approximated by a combination of dipole–induced dipole, dipole–quadrupole, and quadrupole–quadrupole interactions. Surprisingly, different electrostatic components dominate affinity in different enzyme–inhibitor pairs.

## Introduction

The C–F bond is rarely encountered in natural products biosynthesis. Although plants generally contain trace amounts of fluorine absorbed from the soil<sup>1</sup> (presumably as the fluoride ion, F<sup>−</sup>), only a handful of plants are known to utilize fluorine in biosynthesis. The first fluorinated natural product to be identified was fluoroacetate from the tropical plant *Dichapetalum cymosum*.<sup>2</sup> Subsequently, fluoroacetate and its biosynthetic products have been identified in several other plant species. For example, *Dichapetalum toxicarium*, a plant indigenous to southern Africa, contains fluoroacetate and its seeds contain  $\omega$ -fluorinated lipids, presumably derived from the biosynthetic precursor fluoroacetyl-CoA.<sup>3,4</sup> Notably, fluoroacetate is highly toxic to animals because it is converted to fluorocitrate, which inhibits aconitase after displacement of F<sup>−</sup> by OH<sup>−</sup> to form 4-hydroxy-*trans*-aconitate, thus blocking the Krebs cycle.<sup>5–7</sup>

Despite its rare occurrence in biology, the C–F bond is not always a determinant of toxicity and is occasionally exploited

in medicinal chemistry to enhance ligand binding to proteins. Fluorine is the most electronegative element and has a reported van der Waals radius of 1.40–1.47 Å; the van der Waals radius of hydrogen is 1.06–1.20 Å, the precise value depending on the method of measurement.<sup>8</sup> The C–F and C–H bond lengths in saturated hydrocarbons (i.e., of the form C–CH<sub>2</sub>–X) are 1.399 and 1.059 Å, respectively.<sup>9</sup> These dimensions allow for the selective substitution of the C–F group for the C–H group in an organic molecule without significantly increasing the overall size of the molecule. Accordingly, a fluorinated protein ligand should be capable of binding in generally the same location as a nonfluorinated ligand, but the chemical properties of the C–F bond may impact protein–ligand affinity.<sup>10</sup> For example, one strategy is to substitute fluorine for a proton that must be removed in an enzyme reaction mechanism. Since fluorine is not readily removable, the enzyme is effectively inhibited. Thymidylate synthetase is inactivated by 5-fluorouracil deoxyribonucleotide in this manner.<sup>11,12</sup> Another strategy exploits the exceptional electronegativity of fluorine. Introduction of the C–F group adjacent to a ketone carbonyl group enhances the electrophilicity of the ketone, so much so that the fluorinated molecule can bind to a hydrolytic enzyme as a covalent adduct with an active site nucleophile, effectively binding as a transition state analogue.<sup>13</sup>

<sup>†</sup> University of Pennsylvania.

<sup>‡</sup> Swarthmore College.

<sup>⊥</sup> University of California, San Francisco.

<sup>||</sup> University of Michigan.

<sup>\*</sup> University of California, Berkeley.

(1) Bollard, E. G.; Butler, G. W. *Annu. Rev. Plant Physiol.* **1966**, *17*, 77–112.

(2) Marais, J. S. C. *Onderstepoort J. Vet. Sci. Anim. Ind.* **1944**, *20*, 67.

(3) Ward, P. F. V.; Hall, R. J.; Peters, R. A. *Nature* **1964**, *201*, 611–612.

(4) Harper, D. B.; Hamilton, J. T. G.; O'Hagan, D. *Tetrahedron Lett.* **1990**, *31*, 7661–7662.

(5) Morrison, J. F.; Peters, R. A. *Biochem. J.* **1954**, *56*, 473–479.

(6) Lauble, H.; Kennedy, M. C.; Emptage, M. H.; Beinert, H.; Stout, C. D. *Proc. Natl. Acad. Sci. U.S.A.* **1996**, *93*, 13699–13703.

(7) Peters, R.; Wakelin, R. W.; Buffa, P.; Thomas, L. C. *Proc. R. Soc. London Ser. B* **1953**, *140*, 497–507.

(8) Bondi, A. J. *Phys. Chem.* **1964**, *68*, 441–451.

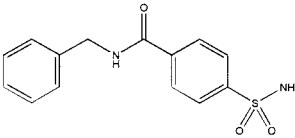
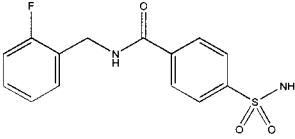
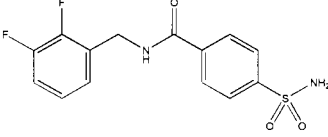
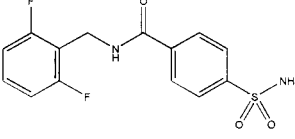
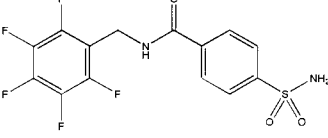
(9) Lide, D. R. *CRC Handbook of Chemistry and Physics*, 80th ed.; CRC: Boca Raton, FL, 1999.

(10) Abeles, R. H.; Alston, T. A. *J. Biol. Chem.* **1990**, *265*, 16705–16708.

(11) Heidelberger, C.; Danenberg, P. V.; Moran, R. G. *Adv. Enzymol.* **1983**, *54*, 58–119.

(12) Pellino, A. M.; Danenberg, P. V. *J. Biol. Chem.* **1985**, *260*, 10996–11000.

**Table 1.** Fluorinated CAII Inhibitors

Inhibitor	$K_d$ (nM) <sup>a,b</sup> native	$K_d$ (nM) <sup>b</sup> Phe-131→Val
 4-(aminosulfonyl)-N-phenylmethylbenzamide (SBB)	2.1	5.6
 4-(aminosulfonyl)-N-[(2-fluorophenyl)methyl]-benzamide (2-fluoro-SBB)	0.36	2.3
 4-(aminosulfonyl)-N-[(2,3-difluorophenyl)methyl]-benzamide (2,3-difluoro-SBB)	0.29	1.6
 4-(aminosulfonyl)-N-[(2,6-difluorophenyl)methyl]-benzamide (2,6-difluoro-SBB)	0.91	3.9
 4-(aminosulfonyl)-N-[(2,3,4,5,6-pentafluorophenyl)methyl]-benzamide (2,3,4,5,6-pentafluoro-SBB)	1.5	2.0

<sup>a</sup> Reference 20. <sup>b</sup> Reference 25.

Fluorinated aromatic rings are particularly interesting because substitution of electronegative fluorine for electropositive hydrogen atoms significantly modulates the electronic properties of the aromatic ring.<sup>14</sup> To illustrate, the quadrupole moment of benzene is  $-29.0 \times 10^{-40} \text{ C}\cdot\text{m}^2$ .<sup>15,16</sup> The magnitude of this negative moment results from delocalized negative charge above and below the plane of the aromatic ring, while the ring hydrogen atoms each have a net charge of +0.15e. However, the quadrupole moment of hexafluorobenzene,  $31.7 \times 10^{-40} \text{ C}\cdot\text{m}^2$ , is essentially equal in magnitude but opposite in sign to that of benzene.<sup>15</sup> The electronegative fluorine atoms inductively polarize the electronic charge distribution so much that a positive electrostatic potential exists above and below the ring, with corresponding negative electrostatic potential around the periphery. Notably, the physical dimensions of benzene and hexafluorobenzene are roughly similar, since the C–H bond

length in benzene is  $1.101 \pm 0.005 \text{ \AA}$  and the C–F bond length in hexafluorobenzene is  $1.327 \pm 0.007 \text{ \AA}$ .<sup>17,18</sup>

Here we report structure–affinity relationships for the binding of a series of fluoroaromatic ligands to a protein host. Specifically, we have studied the complexes between the zinc metalloenzyme carbonic anhydrase II (CAII) and fluorinated derivatives of the inhibitor 4-(aminosulfonyl)-N-phenylmethylbenzamide (SBB; Table 1).<sup>19,20</sup> CAII catalyzes the hydration of carbon dioxide to yield bicarbonate ion and a proton. While the dissociation constant ( $K_d$ ) of SBB is 2.1 nM, various fluorine substitution patterns on its aromatic benzyl group modulate enzyme–inhibitor affinity by a factor of 10.<sup>20,21</sup> The crystal structure of the CAII-SBB complex reveals an edge-to-face interaction between Phe-131 and the benzyl ring of SBB (centroid–centroid separation of 5.9 Å), suggesting a weak but favorable electrostatic attraction between the electronic qua-

(13) Gelb, M. H.; Svaren, J. P.; Abeles, R. H. *Biochemistry* **1985**, *24*, 1813–1817.

(14) Williams, J. H. *Acc. Chem. Res.* **1993**, *26*, 593–598.

(15) Battaglia, M. R.; Buckingham, A. D.; Williams, J. H. *Chem. Phys. Lett.* **1981**, *78*, 421–423.

(16) Coulomb·meter<sup>2</sup> (C·m<sup>2</sup>) is the SI unit of the molecular quadrupole moment. Quadrupole moments are also expressed in buckinghams, where 1 buckingham =  $3.33 \times 10^{-40} \text{ C}\cdot\text{m}^2$ .

(17) Tamagawa, K.; Iijima, T.; Kimura, M. *J. Mol. Struct.* **1976**, *30*, 243–253.

(18) Almenningen, A.; Bastiansen, O.; Seip, R.; Seip, H. M. *Acta Chem. Scand.* **1964**, *18*, 2115–2124.

(19) Cappelalonga Bunn, A. M.; Alexander, R. S.; Christianson, D. W. *J. Am. Chem. Soc.* **1994**, *116*, 5063–5068.

(20) Jain, A.; Whitesides, G. M.; Alexander, R. S.; Christianson, D. W. *J. Med. Chem.* **1994**, *37*, 2100–2105.

(21) Doyon, J. B.; Jain, A. *Org. Lett.* **1999**, *1*, 183–185.

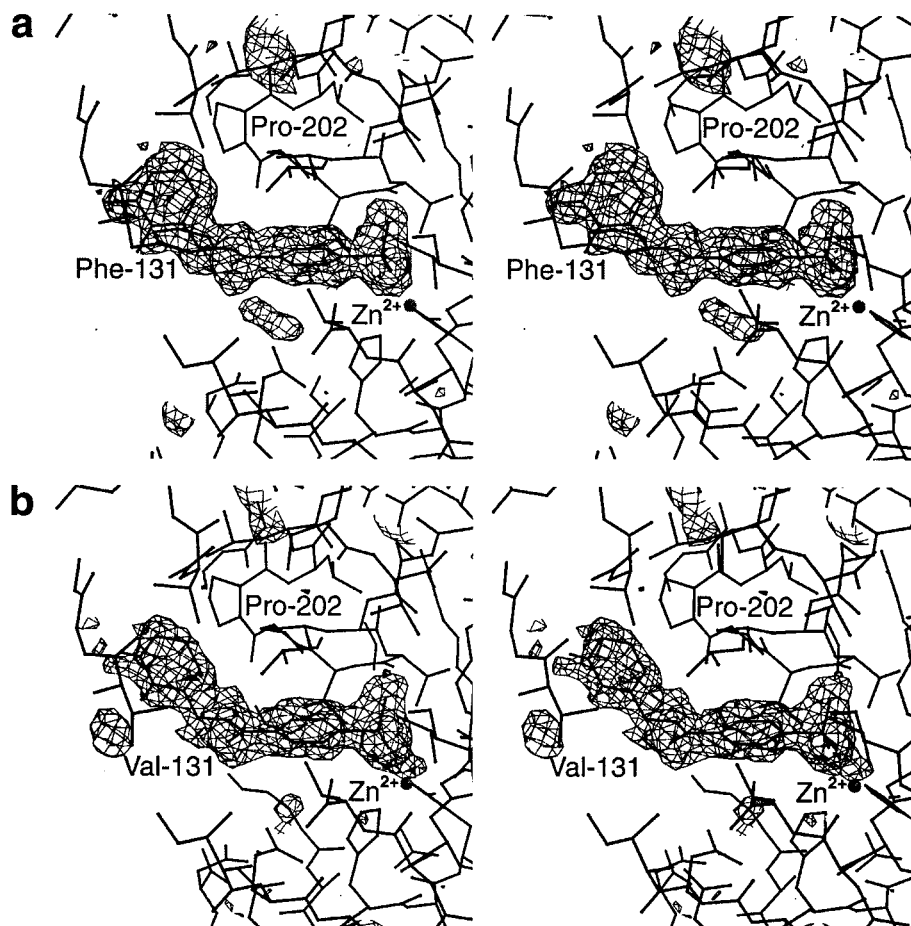
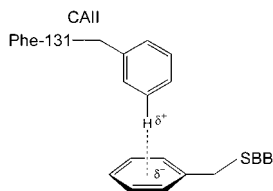


**Figure 1.** Difference electron density maps calculated with Fourier coefficients  $|F_o| - |F_c|$  and phases derived from the final model less the inhibitor and active-site solvent molecules. Both maps are contoured at  $2.0\sigma$ : (a) native CAII-2,3-difluoro-SBB complex,  $K_d = 0.29$  nM; (b) Phe-131→Val CAII-2,3-difluoro-SBB complex,  $K_d = 1.6$  nM. Selected active site residues are indicated.

drupoles of the aromatic rings:<sup>19</sup> the partial positive charge on the ring hydrogen atoms of Phe-131 interacts with the partial negative charge above the ring plane of the inhibitor benzyl group.<sup>14,22</sup> In the sense that this interaction can be viewed as a nonclassical hydrogen bond, the inhibitor aromatic ring is the donor and Phe-131 is the acceptor. The range of centroid–centroid separations observed for such weakly polar interactions<sup>22</sup> is 3.4–6.5 Å, so the CAII–SBB interaction appears to be a textbook example of a quadrupole–quadrupole interaction.



If the quadrupole–quadrupole interaction in the CAII–SBB complex contributes significantly to enzyme–inhibitor affinity, then systematic modulation of aromatic ring electrostatics by fluorine substitution should predictably modulate enzyme–inhibitor affinity. Specifically, increasing fluorine substitution on the benzyl ring of the inhibitor should lead to a repulsive interaction with Phe-131—if the substitution of fluorine for hydrogen is as innocuous as their similar dimensions might imply. On the other hand, if other interactions, e.g., simple van

der Waals interactions, and not quadrupole–quadrupole interactions dominate enzyme–inhibitor affinity, then a different structure–activity relationship should be observed. Accordingly, a library of fluoroaromatic SBB derivatives has been prepared<sup>21,25</sup> and we have determined the X-ray crystal structures of four representative complexes with native CAII at atomic resolution. Additionally, we have determined the structures of five representative complexes with the Phe-131→Val variant of CAII to further probe fluoroaromatic inhibitor interactions with residue-131.<sup>23</sup> Inhibitor structures and affinities are summarized in Table 1.

## Results

The overall structure of CAII remains essentially unchanged upon the binding of each inhibitor, and this is the case for both wild-type and Phe-131→Val CAII. For each fluorinated inhibitor, the interactions of the benzenesulfonamide group with active

(23) Phe-131→Val CAII:  $k_{cat} \times 10^{-5} = 6.6 \pm 0.3$  s<sup>-1</sup>,  $K_M = 9.6 \pm 1.1$  mM,  $k_{cat}/K_M = 6.9 \pm 0.5$  M<sup>-1</sup>s<sup>-1</sup> (CO<sub>2</sub> hydrase activity);  $k_{cat}/K_M = 590 \pm 20$  M<sup>-1</sup>s<sup>-1</sup>,  $pK_a = 7.0 \pm 0.1$  (*p*-nitrophenylacetate hydrolysis); acetazolamide  $K_d = 0.015 \pm 0.003$  μM. Wild-type CAII:  $k_{cat} \times 10^{-5} = 5.9 \pm 0.2$  s<sup>-1</sup>,  $K_M = 12 \pm 1$  mM,  $k_{cat}/K_M = 5.0 \pm 0.2$  M<sup>-1</sup>s<sup>-1</sup> (CO<sub>2</sub> hydrase activity);  $k_{cat}/K_M = 2600 \pm 50$  M<sup>-1</sup>s<sup>-1</sup>,  $pK_a = 7.0 \pm 0.1$  (*p*-nitrophenylacetate hydrolysis); acetazolamide  $K_d = 0.011 \pm 0.002$  μM. See: Nair, S. K.; Krebs, J. F.; Christianson, D. W.; Fierke, C. A. *Biochemistry* **1995**, *34*, 3981–3989.

(24) Gao, J.; Qiao, S.; Whitesides, G. M. *J. Med. Chem.* **1995**, *38*, 2292–2301.

(25) Doyon, J. B.; Hansen, E. A. M.; Kim, C.-Y.; Chang, J. S.; Christianson, D. W.; Madder, R. D.; Voet, J. G.; Baird, T. A., Jr.; Fierke, C. A.; Jain, A. *Org. Lett.* **2000**, *2*, 1189–1192.

(22) Burley, S. K.; Petsko, G. A. *Adv. Protein Chem.* **1988**, *39*, 125–189.

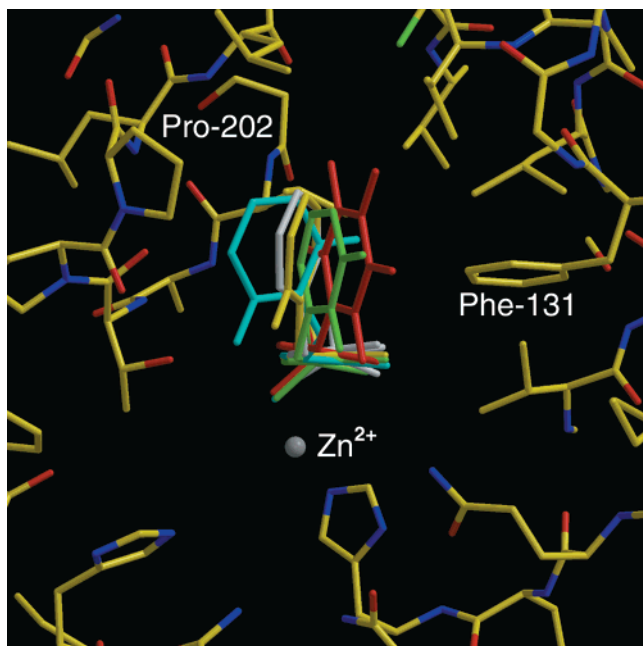


**Figure 2.** Superposition of enzyme–inhibitor complexes; for clarity, only the coordinates of CAII in the CAII–SBB complex are shown (carbon = yellow, nitrogen = blue, oxygen = red, sulfur = green). Inhibitors are color coded as follows: SBB, white; 2-fluoro-SBB, yellow; 2,3-difluoro-SBB, green; 2,6-difluoro-SBB, cyan; 2,3,4,5,6-pentafluoro-SBB, red. Note that the aromatic ring of the inhibitor moves closer to Phe-131 as a consequence of fluorination.

site residues are identical to those observed in the CAII–SBB complex.<sup>19</sup> The ionized nitrogen of the sulfonamide group coordinates to zinc and displaces the zinc-bound hydroxide ion of the native enzyme. This nitrogen also donates a hydrogen bond to the hydroxyl group of Thr-199. One of the sulfonamide oxygens accepts a hydrogen bond from the backbone NH group of Thr-199, while the other sulfonamide oxygen makes no interactions. To illustrate the quality of the experimentally determined structures, difference electron density maps of 2,3-difluoro-SBB bound to wild-type and Phe-131→Val CAIIs are shown in Figure 1.

For each fluorinated inhibitor, interactions of the fluoroaromatic ring with active site residues in wild-type CAII vary with the degree and pattern of fluorination. These differences likely contribute to the observed variations in binding affinity (Table 1).<sup>21</sup> Surprisingly, the fluoroaromatic ring of each inhibitor generally shifts *closer* to Phe-131 with increasing fluorination (Figure 2). This observation contrasts with the expectation of a repulsive quadrupole–quadrupole interaction between the inhibitor fluoroaromatic ring and Phe-131. Indeed, the fluoroaromatic ring of 2,3,4,5,6-pentafluoro-SBB shifts  $\sim 1$  Å closer to Phe-131 than the nonfluorinated aromatic ring of SBB. Therefore, although aromatic ring quadrupoles may contribute to the binding conformation of this series of inhibitors, this contribution appears to be less significant than other factors such as the optimization of simple van der Waals contact surface area for the slightly larger fluoroaromatic rings.

Fluorine substitution in the inhibitor benzyl group is asymmetric in 2-fluoro-SBB and 2,3-difluoro-SBB, which would allow for two comparable binding conformations related by a 180° rotation of the fluoroaromatic ring (fluorine atom(s) can face either the protein surface or solvent). However, only one of these two possible conformations is observed, and this determination is unambiguous in electron density maps (e.g.,

clear density outlines the fluorine atoms of 2,3-difluoro-SBB in Figure 1). In the CAII complexes with both 2-fluoro-SBB and 2,3-difluoro-SBB, fluorine atoms are directed toward solvent. It is notable that the C–F groups prefer to interact with the more polar milieu of solvent instead of packing against the hydrophobic protein surface.

The binding of 2,6-difluoro-SBB and 2,3,4,5,6-pentafluoro-SBB requires the packing of C–F groups against the protein surface: the fluoroaromatic rings of these inhibitors cannot rotate by 180° to relieve C–F⋯protein interactions. This fact may contribute to the 3–5-fold weaker binding of these inhibitors compared with 2-fluoro-SBB and 2,3-difluoro-SBB (Table 1). The C–F groups of these inhibitors associate with a hydrophobic patch defined by the side chains of Val-135, Leu-198, and Leu-204 (data not shown). The hydrophobicities of hydrocarbons and fluorocarbons are similar after correction for differences in molecular surface area, as determined by microemulsion electrokinetic chromatography (MEEKC).<sup>24,25</sup> It is therefore surprising that the tightest binding fluoroaromatic inhibitors are those that do not bury C–F groups against the Val-135 hydrophobic patch, and instead leave C–F groups exposed to solvent. This difference in binding behavior may arise from electrostatic differences between fluorine substituted on an aromatic ring and fluorine substituted on a simple saturated hydrocarbon.

The native and Phe-131→Val CAII structures are essentially superimposable (data not shown), with an rms deviation of 0.16 Å for 258 C $\alpha$  atoms. No noticeable differences are observed among active site residues except for the substitution of residue-131. Consistent with these results, the Phe-131→Val substitution has little effect on the catalytic efficiency of CO<sub>2</sub> hydration, although  $k_{\text{cat}}/K_{\text{M}}$  for *p*-nitrophenylacetate hydrolysis decreases 5-fold.<sup>2,3</sup> Additionally, the affinities of SBB and its fluorinated analogues decrease up to 6-fold (Table 1).

Since there are essentially no differences between the structures of the wild-type CAII–SBB complex and the Phe-131→Val CAII–SBB complex, removal of the bulky phenyl ring of Phe-131 does not affect the binding conformation of SBB (Figure 3a). However, conformational differences are observed between the complexes of wild-type and Phe-131→Val CAIIs with fluorinated inhibitors. The centroids of inhibitor fluoroaromatic rings do not move closer to, or away from, Val-131. Instead, the fluoroaromatic rings tend to rotate about the C-phenyl bond by +20° (2-fluoro-SBB), +17° (2,3-difluoro-SBB), and –78° (2,6-difluoro-SBB) relative to the conformation of SBB. Superposition of the native CAII–2-fluoro-SBB and Phe-131→Val CAII–2-fluoro-SBB complexes illustrates this rotation (Figure 3b), and the general trend for the inhibitor series is evident in Figure 4. In addition to the fluoroaromatic ring rotation, the amide bonds of 2,6-difluoro-SBB and 2,3,4,5,6-pentafluoro-SBB deviate from ideal planarity by 22° and 26°, respectively, and this deviation presumably compromises affinity.

Surprisingly, 2:1 inhibitor binding is observed in the structure of 2,3,4,5,6-pentafluoro-SBB complexed with Phe-131→Val CAII (Figures 4 and 5). One inhibitor molecule binds in the hydrophobic cleft with its sulfonamide nitrogen coordinated to zinc in the usual manner. A second molecule binds at the entrance to the hydrophobic cleft where additional binding surface is created by the Phe-131→Val substitution. The sulfonamide nitrogen atom of this second inhibitor molecule donates a hydrogen bond to Asp-72. No other hydrogen bonds, either direct or water-mediated, are made with the protein. The secondary binding site is a hydrophobic cleft formed as a consequence of the Phe-131→Val substitution and crystal lattice



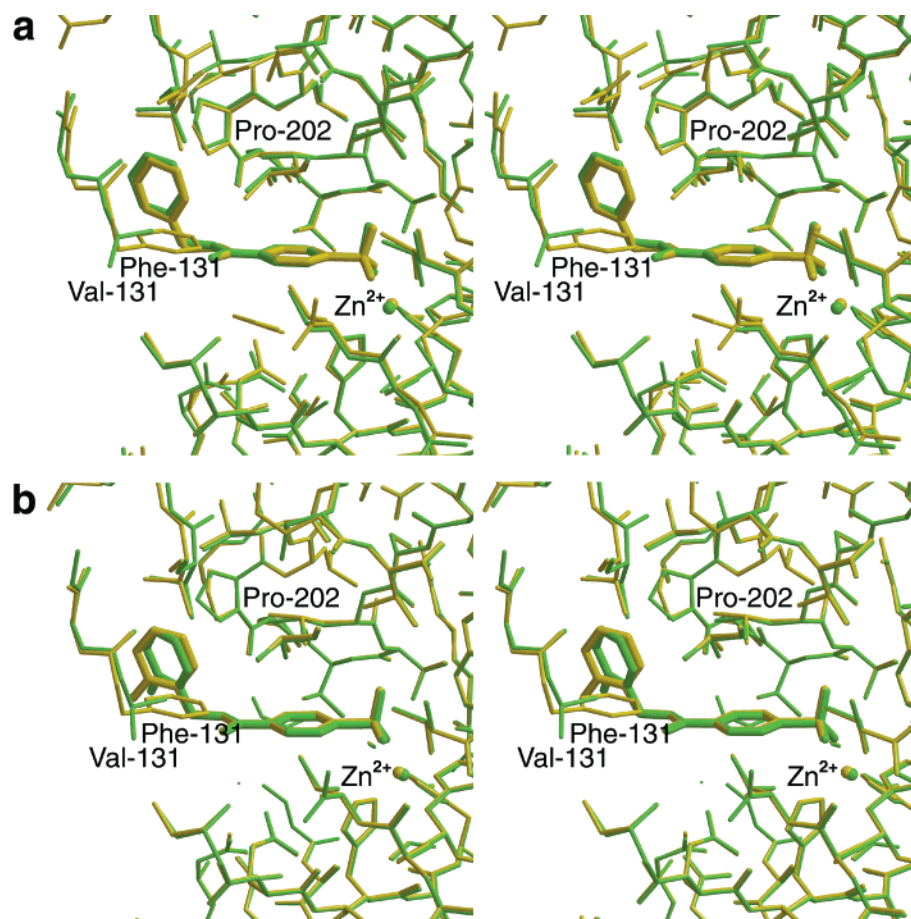


**Figure 3.** (a) Superposition of native CAII-SBB (yellow) and Phe-131→Val CAII-SBB (green) complexes. (b) Superposition of native CAII-2-fluoro-SBB (yellow) and Phe-131→Val CAII-2-fluoro-SBB (green) complexes. Selected active site residues are indicated. Note that inhibitors are drawn with thicker bonds.

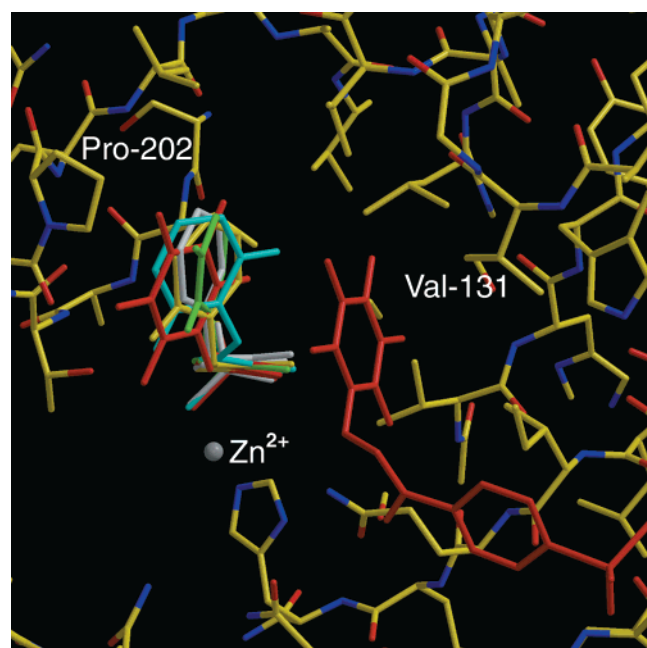
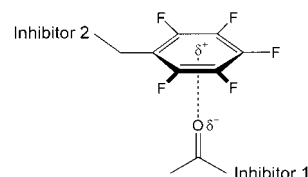


**Figure 4.** Superposition of enzyme–inhibitor complexes; for clarity, only the coordinates of Phe-131→Val CAII in the Phe-131→Val CAII-SBB complex are shown (carbon = yellow, nitrogen = blue, oxygen = red, sulfur = green). Inhibitors are color coded as follows: SBB, white; 2-fluoro-SBB, yellow; 2,3-difluoro-SBB, green; 2,6-difluoro-SBB, cyan; 2,3,4,5,6-pentafluoro-SBB, red.

packing of the CAII molecules at positions  $x, y, z$  and  $-x, y + 1/2, -z$  (Figure 6). Such 2:1 binding is not observed in any of

the native CAII-inhibitor complexes because the hydrophobic cleft in the crystal lattice is occluded by the bulky Phe-131 side chain. A single inhibitor molecule binds to Phe-131→Val CAII in solution (data not shown), suggesting that the interaction with the primary CAII molecule is not sufficient by itself to bind the second inhibitor with appreciable affinity. Interestingly, phenol also binds to human CAII with a 2:1 ratio.<sup>26</sup> The first phenol molecule binds in the hydrophobic pocket of the active site and displaces a water molecule. The second molecule makes a hydrogen bond with Asp-72, the same residue that forms a hydrogen bond with 2,3,4,5,6-pentafluoro-SBB in the Phe-131→Val CAII.

Interestingly, the pentafluorobenzyl ring of the second inhibitor molecule makes a quadrupole–dipole interaction with the carbonyl oxygen of the first inhibitor molecule (the ring centroid–oxygen distance is 2.9 Å). A comparable electrostatic



interaction is not feasible for the binding of SBB, 2-fluoro-SBB, or 2,6-difluoro-SBB because the charge distribution of the aromatic ring is such that there is partial negative charge

(26) Nair, S. K.; Ludwig, P. A.; Christianson, D. W. *J. Am. Chem. Soc.* **1994**, *116*, 3659–3660.

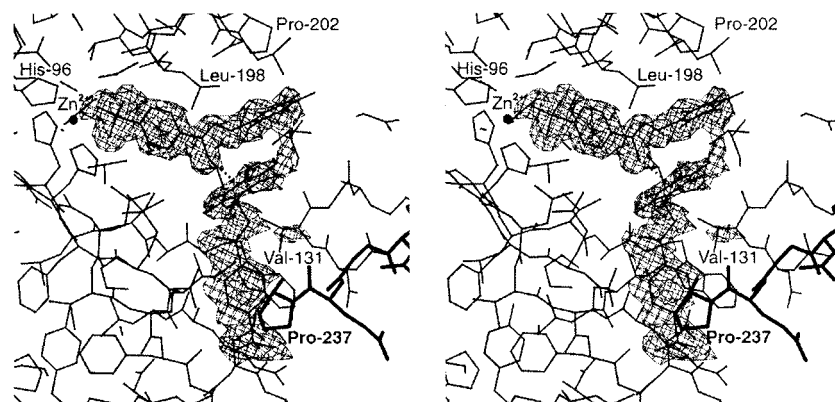


**Figure 5.** Difference electron density map (contoured at  $3.2\sigma$ ) of Phe-131→Val CAII-2,3,4,5,6-pentafluoro-SBB complex ( $K_d = 2.0$  nM), calculated with Fourier coefficients  $|F_o| - |F_c|$  and phases derived from the final model less the inhibitor and active-site solvent molecules. The symmetry-related CAII molecule is shown in thick bonds. Selected residues are indicated. A dashed line highlights the dipole–quadrupole interaction between the carbonyl oxygen of the first inhibitor molecule and the fluoroaromatic ring of the second inhibitor molecule.

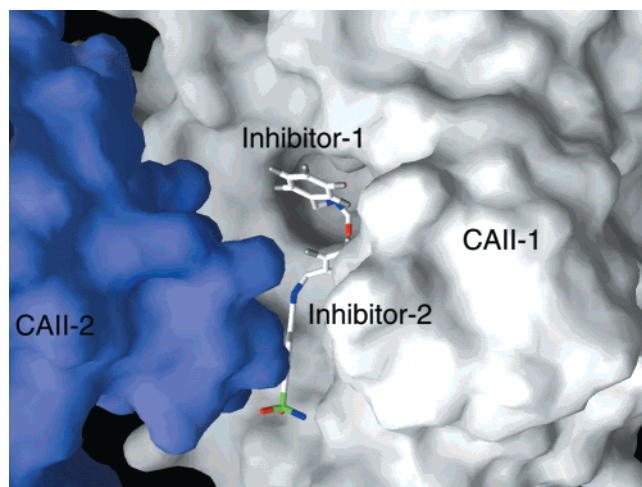
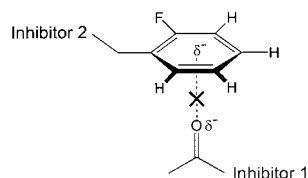


**Figure 6.** Phe-131→Val CAII-2,3,4,5,6-pentafluoro-SBB complex. Inhibitor-1 binds in the active site of CAII-1. Inhibitor-2 binds in a cleft formed by the CAII-1/CAII-2 interface in the crystal lattice. CAII-2 is located at position  $-x, y + 1/2, -z$  relative to CAII-1.

above and below the plane of the ring. This would result in a repulsive interaction with a second inhibitor molecule.



## Discussion

Affinity differences in this series of inhibitors are subtle, ranging within a factor of 7.2 for wild-type CAII and within a factor of 19.3 between wild-type and Phe-131→Val CAIIs (Table 1). These affinity differences must arise from differences in the degree and pattern of fluorine substitution in the benzyl ring alone, since each inhibitor shares an identical benzene-sulfonamide core. One possible factor contributing to enzyme–inhibitor affinity is the inductive effect of electronegative fluorine atoms on the sulfonamide acidity. However, sulfonamide  $pK_a$  values are not perturbed significantly by the fluoro-benzyl ring. Specifically, no difference is evident between the  $pK_a$  values of SBB and 2,3,4,5,6-pentafluoro-SBB when the pH-dependent absorbance change at 260 nm is monitored.

Likewise, no difference is expected for the  $pK_a$  values of SBB derivatives bearing intermediate fluorine substitution patterns.

Contact surface area is another contributing factor to enzyme–inhibitor affinity, where the linear free energy relationship  $\Delta G = 0.02 \text{ kcal}/(\text{mol } \text{Å}^2)$  provides a useful estimate for nonpolar association interactions.<sup>27</sup> In our inhibitor series, however, no correlation is observed between affinity and contact surface area (Table 4). This suggests that contact surface area is not the sole determinant of enzyme–inhibitor affinity in this series of inhibitors.

In the Phe-131→Val CAII-inhibitor complexes, Pro-202 interacts most closely with the inhibitor fluoroaromatic ring; accordingly, the observed affinity differences should be attributable largely to this interaction. If the fluoroaromatic ring contact surface area does not dominate enzyme–inhibitor affinity differences, then what inhibitor property does? Surprisingly, there is a noticeable correlation between affinity and dipole moment of the inhibitor aromatic ring (Figure 7; electric moments are approximated by fluorine-substituted benzene in Table 5). Since the Pro-202 side chain is nonpolar, its electrostatic interaction with the fluoroaromatic ring of the inhibitor is of the dipole–induced dipole type. Specifically, the fluoroaromatic ring of the inhibitor with dipole moment  $\mu_1$  induces an attractive dipole moment  $\mu_2$  in the nonpolar partner, Pro-202. The average interaction energy for a dipole–induced dipole pair separated by distance  $r_1$  is

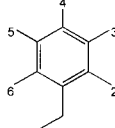
$$V = - \frac{(3 \cos^2 \theta + 1) \mu_1^2 \alpha_2}{16\pi^2 \epsilon 2r_1^6} \quad (1)$$

$\theta$  is the angle between the dipole moment and the AB segment (A is Pro-202 centroid and B is the inhibitor aromatic ring centroid),  $\mu_1$  is the permanent dipole moment of molecule 1,  $\alpha_2$  is the polarizability of molecule 2, and  $\epsilon$  is the permittivity of the medium.<sup>28</sup> Using the centroid–centroid separation between the inhibitor fluoroaromatic ring and Pro-202, we can establish a linear free energy relationship based on the dipole moment of the fluoroaromatic ring of the inhibitor (Table 6, Figure 8). The correlation is quite good ( $r^2 = 0.8292$ ) and we conclude that the observed affinity trend in the Phe-131→Val CAII-inhibitor complexes is dominated by the dipole–induced dipole interaction.

(27) Radzicka, A.; Wolfenden, R. *Biochemistry* **1988**, *27*, 1664–1670.

(28) Daune, M. *Molecular Biophysics: Structures in Motion*; Oxford University Press: Oxford; New York, 1999.

**Table 2.** Data Collection and Refinement Statistics for Wild-Type CAII-Inhibitor Complexes

SBB fluorine substitution pattern 	2	2,3	2,6	2,3,4,5,6
Number of measured reflections	103,002	137,502	114,180	124,289
Number of unique reflections	16,135	22,122	17,661	19,463
Maximum resolution (Å)	2.04	1.80	1.94	1.86
$R_{\text{merge}}^a$	0.070	0.077	0.053	0.085
Completeness of data (%)	99.8	94.3	94.1	91.4
Number of reflections used in refinement ( $>2\sigma$ )	15,842	18,908	16,067	18,373
Number of reflections in $R_{\text{free}}$ test set	771	959	784	920
$R_{\text{cryst}}^b$	0.198	0.165	0.198	0.182
$R_{\text{free}}^c$	0.277	0.215	0.262	0.239
Number of nonhydrogen atoms <sup>d</sup>	2,081	2,082	2,082	2,085
Number of solvent molecules included in refinement	99	83	138	71
RMSD from ideal bond lengths (Å)	0.009	0.009	0.009	0.008
RMSD from ideal bond angles (°)	1.6	1.6	1.6	1.7
RMSD from ideal dihedral angles (°)	25.0	24.9	25.0	24.8
RMSD from ideal improper angles (°)	1.4	1.3	1.4	1.3
RCSB accession code	1G1D	1G52	1G53	1G54

<sup>a</sup>  $R_{\text{merge}}$  for replicate reflections,  $R = \sum |I_h - \langle I_h \rangle| / \sum \langle I_h \rangle$ ;  $I_h$  = intensity measured for reflection  $h$ ;  $\langle I_h \rangle$  = average intensity for reflection  $h$  calculated from replicate data. <sup>b</sup> Crystallographic  $R$  factor,  $R_{\text{cryst}} = \sum ||F_o| - |F_c|| / \sum |F_o|$ ;  $|F_o|$  and  $|F_c|$  are the observed and calculated structure factor amplitudes, respectively, for those reflections not included in the  $R_{\text{free}}$  test set. <sup>c</sup> Free  $R$  factor,  $R_{\text{free}} = \sum ||F_o| - |F_c|| / \sum |F_o|$  for only those reflections included in the  $R_{\text{free}}$  test set. <sup>d</sup> In asymmetric unit.

In the native CAII-inhibitor complexes, the inhibitor aromatic ring can interact with both Pro-202 and Phe-131 (Table 4). As proposed for the Phe-131→Val CAII-inhibitor complexes, the interaction between Pro-202 and the fluoroaromatic ring of the inhibitor is that of a dipole–induced dipole attraction. However, the correlation between the dipole moment of the fluoroaromatic ring and inhibitor affinity is weaker for native CAII-inhibitor complexes (Figure 7). Could higher-order electrostatic interactions with Phe-131 affect binding to the native enzyme? Phe-131 has a large permanent quadrupole moment that can interact favorably with the inhibitor fluoroaromatic ring, as discussed in the Introduction. However, a fluoroaromatic ring has both a permanent dipole moment and a permanent quadrupole moment, so two separate electrostatic interactions must be considered. First, the inhibitor dipole–Phe-131 quadrupole interaction has an average potential energy  $V$  described by the simplified equation

$$V \propto - \frac{\mu_1 Q_2}{4\pi\epsilon r_2^4} \quad (2)$$

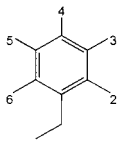
where  $\mu_1$  is the dipole moment of the inhibitor ring,  $Q_2$  is the magnitude of the quadrupole moment of the Phe-131 side chain, and  $r_2$  is the centroid–centroid separation between the fluoroaromatic ring of the inhibitor and Phe-131. This interaction is also always favorable, and in our case it is independent of the

direction of the dipole moment vector since the edge-to-face geometry between inhibitor ring and Phe-131 is always maintained (Figure 2). Second, the interaction between the fluoroaromatic ring quadrupole moment and that of Phe-131 has an average potential energy of

$$V \propto \frac{Q_1 Q_2}{4\pi\epsilon r_2^5} \quad (3)$$

where  $Q_1$  and  $Q_2$  are the quadrupole moments of the inhibitor fluoroaromatic ring and Phe-131, respectively, and  $r_2$  is the centroid–centroid separation. Note that the sign of the term depends on the sign of the two quadrupole moments. In an edge-to-face geometry the two aromatic rings attract one another when the signs of the quadrupole moment are the same. In a face-to-face interaction, the aromatic rings interact favorably when the signs of the quadrupole moment are opposite. The quadrupole–quadrupole interaction energy is dependent on the angle between the two interacting rings, but in our case the edge-to-face geometry is conserved throughout the series (Figure 2). Therefore, for this series of inhibitors the potential energy equation is simplified to (3), with the only variable being  $Q_1$ , the magnitude of the quadrupole moment of the inhibitor fluoroaromatic ring. We can derive a linear structure–activity relationship with  $r^2 = 0.8292$  for inhibitor binding to native CAII by combining the terms (1), (2), and (3), which reflects

**Table 3.** Data Collection and Refinement Statistics for Phe-131→Val CAII-inhibitor complexes

SBB fluorine substitution pattern 	Phe-131→Val CAII (native)	perhydro (SBB)	2	2,3	2,6	2,3,4,5,6
Number of measured reflections	123,239	113,167	128,565	126,272	123,953	131,410
Number of unique reflections	21,142	18,565	21,161	19,837	19,523	21,422
Maximum resolution (Å)	1.86	1.96	1.83	1.84	1.86	1.84
$R_{\text{merge}}^a$	0.057	0.112	0.202	0.082	0.086	0.061
Completeness of data (%)	91.6	94.7	94.5	90.0	91.6	90.0
Number of reflections used in refinement ( $>2\sigma$ )	18,209	16,084	17,900	18,870	18,256	20,577
Number of reflections in $R_{\text{free}}$ test set	932	824	939	941	922	1019
$R_{\text{cryst}}^b$	0.182	0.197	0.181	0.185	0.178	0.183
$R_{\text{free}}^c$	0.234	0.284	0.239	0.236	0.239	0.233
Number of nonhydrogen atoms <sup>d</sup>	2,056	2,076	2,077	2,078	2,078	2,106
Number of solvent molecules included in refinement	184	132	172	129	183	173
RMSD from ideal bond lengths (Å)	0.008	0.009	0.008	0.008	0.008	0.008
RMSD from ideal bond angles (°)	1.6	1.5	1.5	1.5	1.5	1.5
RMSD from ideal dihedral angles (°)	25.1	25.2	24.7	24.9	24.6	24.5
RMSD from ideal improper angles (°)	1.3	1.3	1.3	1.4	1.3	1.3
RCSB accession code	1G3Z	1G4O	1G45	1G46	1G48	1G4J

<sup>a</sup>  $R_{\text{merge}}$  for replicate reflections,  $R = \sum |I_h - \langle I_h \rangle| / \sum \langle I_h \rangle$ ;  $I_h$  = intensity measured for reflection  $h$ ;  $\langle I_h \rangle$  = average intensity for reflection  $h$  calculated from replicate data. <sup>b</sup> Crystallographic  $R$  factor,  $R_{\text{cryst}} = \sum ||F_o| - |F_c|| / \sum |F_o|$ ;  $|F_o|$  and  $|F_c|$  are the observed and calculated structure factor amplitudes, respectively, for those reflections not included in the  $R_{\text{free}}$  test set. <sup>c</sup> Free  $R$  factor,  $R_{\text{free}} = \sum ||F_o| - |F_c|| / \sum |F_o|$  for only those reflections included in the  $R_{\text{free}}$  test set. <sup>d</sup> In asymmetric unit.

**Table 4.** Physical Constants for the Enzyme–Inhibitor Complex Series

enzyme	inhibitor	$\Delta G^a$ E + I → EI (kcal/mol)	Pro-202 to inhibitor distance <sup>b</sup> (Å)	Phe-131 to inhibitor distance <sup>c</sup> (Å)	enzyme–inhibitor contact surface area <sup>d</sup> (Å <sup>2</sup> )
native	SBB	−11.80	4.94	5.92	292.31
native	2-fluoro-SBB	−12.84	5.16	5.95	296.96
native	2,3-difluoro-SBB	−12.97	5.75	5.51	299.14
native	2,6-difluoro-SBB	−12.30	4.79	6.76	261.62
native	2,3,4,5,6-pentafluoro-SBB	−12.00	6.53	5.08	290.53
Phe-131→Val	SBB	−11.22	4.82		279.44
Phe-131→Val	2-fluoro-SBB	−11.75	4.95		281.31
Phe-131→Val	2,3-difluoro-SBB	−11.96	5.05		274.10
Phe-131→Val	2,6-difluoro-SBB	−11.44	4.88		289.18
Phe-131→Val	2,3,4,5,6-pentafluoro-SBB	−11.83	5.14		266.43

<sup>a</sup>  $\Delta G$  is derived from experimental  $K_d$  values (Table 1). <sup>b</sup> Distance is from Pro-202 centroid to inhibitor aromatic ring centroid. <sup>c</sup> Distance is from Phe-131 centroid to inhibitor aromatic ring centroid. <sup>d</sup> Contact surface area ( $A_{\text{contact}}$ ) is calculated with the relationship  $A_{\text{contact}} = (A_E + A_I - A_{\text{EI}})/2$ , where  $A_E$ ,  $A_I$ , and  $A_{\text{EI}}$  represent the solvent-accessible surface area of the native enzyme, inhibitor, and enzyme–inhibitor complex, respectively. Solvent-accessible areas were calculated using GRASP<sup>40</sup> with a probe radius of 1.4 Å.

the contribution of dipole–induced dipole interactions with Pro-202, dipole–quadrupole interactions with Phe-131, and quadrupole–quadrupole interactions with Phe-131, respectively (Figure 8). It is notable that the subtle structure–affinity trends in this series of inhibitors can be approximated by a simplified

electrostatics expression; that the slope of the regression line is 1 further validates the approximation.

It is worthwhile to look more closely at the calculated values of the terms involved in the proposed structure–activity relationship. The equation describing all enzyme–inhibitor



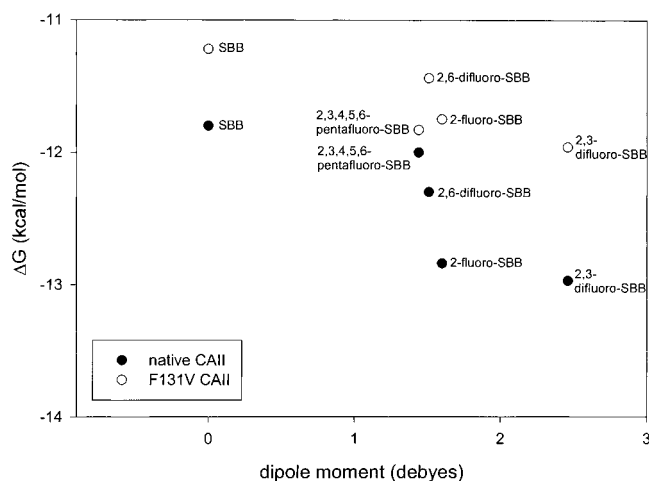


**Figure 7.** Free energy dependence of enzyme–inhibitor binding on the dipole moment of the fluoroaromatic ring. Dipole moments are experimental values of benzene, fluorobenzene, 1,2-difluorobenzene, 1,3-difluorobenzene, and 1,2,3,4,5-pentafluorobenzene.<sup>9,42</sup>

**Table 5.** Electric Moments of the Inhibitor Benzyl Ring

inhibitor	dipole moment <sup>a</sup> (debye)	quadrupole moment <sup>a</sup> ( $Q_{zz}$ , <sup>c</sup> buckingham)
SBB	0.00 <sup>b</sup>	-8.56 <sup>d</sup>
2-fluoro-SBB	1.60 <sup>b</sup>	-6.33 <sup>d</sup>
2,3-difluoro-SBB	2.46 <sup>b</sup>	-4.60 <sup>d</sup>
2,6-difluoro-SBB	1.51 <sup>b</sup>	-3.17 <sup>d</sup>
2,3,4,5,6-pentafluoro-SBB	1.44 <sup>c</sup>	6.11 <sup>d</sup>

<sup>a</sup> Dipole and quadrupole moments are those of benzene, fluorobenzene, 1,2-difluorobenzene, 1,3-difluorobenzene, and 1,2,3,4,5-pentafluorobenzene, respectively. <sup>b</sup> Reference 9. <sup>c</sup> Reference 41. All dipole moments are experimental values. <sup>d</sup> Reference 42. All quadrupole moments are from ab initio calculations. <sup>e</sup> All molecules are centered on their centers of mass, and the z-axis is perpendicular to the aromatic ring.

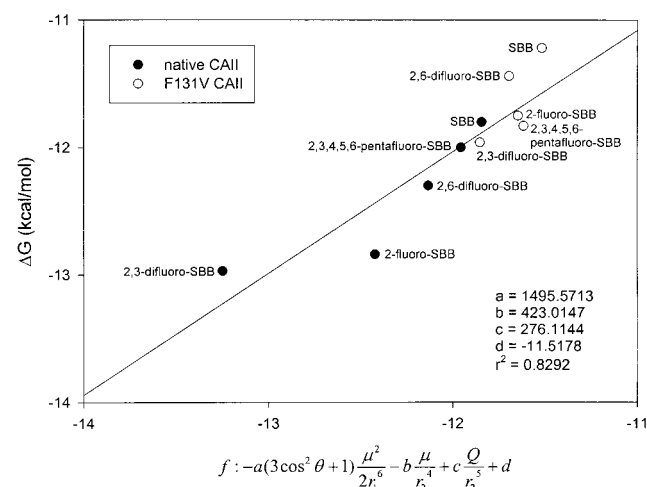


**Figure 8.** Structure–activity relationship describing the binding of fluoroaromatic inhibitors to wild-type and Phe-131→Val CAIIs.

combinations is

$$f: -a(3\cos^2 + 1)\frac{\mu^2}{2r_1^6} - b\frac{\mu}{r_2^4} + c\frac{Q}{r_3^5} + d,$$

$$a = 1495.57, b = 423.01, c = 276.11, d = -11.52 \quad (4)$$

The calculated values for individual terms of eq 4 are listed in Table 6. Weakly polar interactions contribute significantly, and sometimes dominate, structure–affinity relationships. For ex-

ample, the quadrupole–quadrupole interaction is favorable in all cases except for 2,3,4,5,6-pentafluoro-SBB; for this inhibitor, the third term of eq 4 has a positive value, indicating the expected repulsive interaction where the positive electrostatic potential of the inhibitor ring face repels the positive electrostatic potential around the circumference of Phe-131. However, despite this unfavorable quadrupole–quadrupole interaction, the pentafluoroaromatic ring of the inhibitor moves toward Phe-131 (Figure 2) to maximize the dipole–quadrupole interaction. Free energy values listed in Table 6 show that the unfavorable quadrupole–quadrupole interaction is more than compensated by the favorable dipole–quadrupole interaction in the native CAII-2,3,4,5,6-pentafluoro-SBB complex.

Electrostatic arguments do not explain the orientation of fluorine atoms toward solvent in the CAII complexes with 2-fluoro-SBB and 2,3-difluoro-SBB. Ordinarily, the relatively hydrophobic fluorine atoms would be expected to pack against the hydrophobic protein surface. However, analysis of the structures indicates that the 2-fluoro substituents are directed toward solvent to avoid an unfavorable electrostatic interaction with the inhibitor carbonyl oxygen atom. In the native CAII-2-fluoro-SBB complex structure, the F...O distance is 5.37 Å. If the fluoroaromatic ring of 2-fluoro-SBB were rotated by 180°, the distance between these electronegative atoms would be 2.84 Å and a repulsive interaction would result. In the CAII complexes with 2,6-difluoro-SBB and 2,3,4,5,6-pentafluoro-SBB, this unfavorable electrostatic repulsion cannot be avoided by rotating the fluoroaromatic ring by 180°. Instead, the amide bond deviates from ideal planarity by 22–27° to relieve some of the F...O repulsion (native CAII-2,6-difluoro-SBB, Phe-131→Val CAII-2,6-difluoro-SBB, Phe-131→Val CAII-2,3,4,5,6-pentafluoro-SBB).

## Conclusions

New designs of CAII inhibitors have great significance in ophthalmology. Inhibition of CAII in the eye lowers intraocular pressure in glaucoma patients; accordingly, novel and tight-binding CAII inhibitors are potentially useful in glaucoma therapy.<sup>29–31</sup> In the current work, we have demonstrated that a tight-binding inhibitor can be improved even further by simply substituting fluorine for hydrogen at strategic location(s) to enhance weakly polar interactions with adjacent enzyme residues. Strikingly, the structural basis of variations in affinity can be simplified to a combination of dipole–induced dipole, dipole–quadrupole, and quadrupole–quadrupole interactions between the fluoroaromatic inhibitors summarized in Table 1 and just two residues in the CAII active site: Pro-202 and Phe-131. In different enzyme–inhibitor pairs, different electrostatic effects dominate affinity as evident in Table 6. Thus, neither quadrupole–quadrupole nor London interactions dominate the series, and an unanticipated contribution from the fluoroaromatic ring dipole moment is revealed. In an aromatic–aromatic pair comprising a molecular torsion balance, London forces dominate over electrostatic interactions and this result is considered within the greater context of macromolecular aromatic–aromatic interactions.<sup>32</sup> However, although this conclusion is valid for the specific system studied, our results show that within the context of a macromolecule–ligand interaction, distinct electrostatic effects can dominate affinity on a case by case basis.

(29) Friedenwald, J. S. *Am. J. Ophthalm.* **1949**, *32*, 9–27.

(30) Kinsey, V. E. *Arch. Ophthalm.* **1953**, *50*, 401–417.

(31) Maren, T. H. *Drug Dev. Res.* **1987**, *10*, 255–276.

(32) Kim, E.-I.; Paliwal, S.; Wilcox, C. S. *J. Am. Chem. Soc.* **1998**, *120*, 11192–11193.

**Table 6.** Values of Functional Terms for CAII-inhibitor Complexes [ $f = a(3 \cos^2 \theta + 1)(\mu^2/2r_1^6) - b(\mu/r_2^4) + c(Q/r_2^5) + d$ ;  $a = 1495.5713$ ,  $b = 423.0147$ ,  $c = 276.1144$ ,  $d = -11.5178$ ]

enzyme	inhibitor	Term 1 $-a(\mu^2/2r_1^6) \cdot$ $(3 \cos^2 \theta + 1)$	Term 2 $-b(\mu/r_2^4)$	Term 3 $c(Q/r_2^5)$	Term 4 $d$	$f$
native CAII	SBB	0.00	0.00	-0.33	-11.52	-11.84
native CAII	2-fluoro-SBB	-0.13	-0.54	-0.23	-11.52	-12.42
native CAII	2,3-difluoro-SBB	-0.35	-1.13	-0.25	-11.52	-13.25
native CAII	2,6-difluoro-SBB	-0.25	-0.31	-0.06	-11.52	-12.13
native CAII	2,3,4,5,6-pentafluoro-SBB	-0.02	-0.91	0.50	-11.52	-11.96
F131V CAII	SBB	0.00	0.00	0.00	-11.52	-11.52
F131V CAII	2-fluoro-SBB	-0.13	0.00	0.00	-11.52	-11.66
F131V CAII	2,3-difluoro-SBB	-0.34	0.00	0.00	-11.52	-11.88
F131V CAII	2,6-difluoro-SBB	-0.18	0.00	0.00	-11.52	-11.71
F131V CAII	2,3,4,5,6-pentafluoro-SBB	-0.10	0.00	0.00	-11.52	-11.63

<sup>a</sup>  $r_1$  and  $r_2$  are the centroid-centroid separations between the inhibitor ring and Pro-202 and Phe-131, respectively;  $\mu$  is the dipole moment of the inhibitor ring;  $Q$  is the quadrupole moment of the inhibitor ring.

## Experimental Section

The Phe-131→Val substitution was introduced using oligonucleotide-directed mutagenesis of pACA which encodes wild-type CAII.<sup>33,34</sup> The presence of the desired mutation was verified by sequencing the entire CAII gene using the method of Sanger and colleagues.<sup>35</sup> The initial rate of CO<sub>2</sub> hydration was measured by the changing pH-indicator method<sup>36</sup> in a KinTek stopped-flow apparatus at 6–24 mM CO<sub>2</sub>, 25  $\mu$ M *m*-cresol purple, 50 mM TAPS (*N*-tris[hydroxymethyl]methyl-2-aminopropanesulfonic acid), pH 8.5, 25 °C, 0.1 mM EDTA (ethylenediaminetetraacetic acid) with the ionic strength maintained at 0.1 M with Na<sub>2</sub>SO<sub>4</sub>. The rate constants,  $k_{cat}$  and  $k_{cat}/K_M$ , were determined by fitting the observed initial rates at various substrate concentrations to the Michaelis–Menten equation. The binding constant of acetazolamide (AZA) was determined by competition with dansylamide (DNSA). Phe-131→Val CAII (5–20 nM) was incubated with 0.01–1.0  $\mu$ M DNSA to form E·DNSA and then AZA was added to compete for the binding site to form E·AZA, decreasing the observed fluorescence.

Crystals of recombinant wild-type and Phe-131→Val CAIIs were grown by the hanging drop method. Typically, 5  $\mu$ L of protein solution (8–12 mg/mL of protein, 1 mM methyl mercuric acetate, 50 mM Tris-sulfate, pH 8.0) and 5  $\mu$ L of precipitant buffer (2.60–2.75 M (NH<sub>4</sub>)<sub>2</sub>SO<sub>4</sub>, 50 mM Tris-sulfate, pH 8.0) were combined in a single drop hanging over 1 mL of precipitant buffer at 4 °C. Crystals appeared within 2 weeks and were isomorphous with those of native CAII, belonging to space group *P*2<sub>1</sub> with typical unit cell parameters  $a = 42.7$  Å,  $b = 41.4$  Å,  $c = 72.9$  Å, and  $\beta = 104.5^\circ$ .

Prior to the preparation of crystalline enzyme–inhibitor complexes, CAII crystals were cross-linked by adding 5  $\mu$ L of glutaraldehyde solution (0.8% glutaraldehyde (v/v), 4.0 M (NH<sub>4</sub>)<sub>2</sub>SO<sub>4</sub>, 50 mM Tris-sulfate, pH 8.0) to the hanging drop, allowing it to equilibrate at 4 °C for 72 h. Each crystal was then transferred to a 10  $\mu$ L drop containing a stabilization buffer of 3.5 M (NH<sub>4</sub>)<sub>2</sub>SO<sub>4</sub> and 50 mM Tris-sulfate, pH

(33) Nair, S. K.; Calderone, T. L.; Christianson, D. W.; Fierke, C. A. *J. Biol. Chem.* **1991**, *266*, 17320–17325.

(34) Kunkel, T. A.; Roberts, J. D.; Zakour, R. A. *Methods Enzymol.* **1987**, *367*–382.

(35) Sanger, F.; Nicklen, S.; Coulson, A. R. *Proc. Natl. Acad. Sci. U.S.A.* **1977**, *74*, 5463–5467.

(36) Khalifah, R. G. *J. Biol. Chem.* **1971**, *246*, 2561–2573.

8.0. Finally, 1  $\mu$ L of inhibitor solution (10 mM inhibitor in DMSO) was added to this drop and allowed to equilibrate at 4 °C for 1 week. Inhibitors were synthesized as described<sup>21</sup> and crystals of enzyme–inhibitor complexes were mounted in 0.7 mm glass capillaries.

X-ray diffraction data were collected at room temperature using an R-Axis IIC image plate detector (Molecular Structure Corporation), with a Rigaku RU-200HB rotating anode generator (operating at 50 kV and 100 mA) supplying Cu K $\alpha$  radiation focused with Yale double mirrors. Raw diffraction data were processed using the HKL suite of programs.<sup>37</sup>

The 1.54 Å resolution structure of native human CAII retrieved from the Research Collaboratory for Structural Bioinformatics (RCSB; accession code = 2CBA) was used as the starting coordinate set for the refinement of each enzyme–inhibitor complex structure.<sup>38</sup> Each structure was refined by simulated annealing with energy minimization as implemented in X-PLOR.<sup>39</sup> Inhibitor atoms and active site solvent molecules were added into electron density maps generated with Fourier coefficients  $(2|F_o| - |F_c|)$  and  $(|F_o| - |F_c|)$  and phases calculated from the refined model when the *R*-factor dropped below 0.20. Refinement converged smoothly to final crystallographic *R*-factors within the range 0.165–0.198. Data refinement and collection statistics for wild-type and Phe-131→Val CAIIs are recorded in Tables 2 and 3, respectively. Coordinates of all enzyme–inhibitor complexes have been deposited in the RCSB with accession codes designated in Tables 2 and 3.

**Acknowledgment.** We thank the NIH for grants GM45614 (D.W.C.) and GM40602 (C.A.F.) in support of this work.

JA002627N

(37) Otwinowski, Z.; Minor, W. *Methods Enzymol.* **1997**, *276*, 307–326.

(38) Håkansson, K.; Carlsson M.; Svensson L. A.; Liljas, A. *J. Mol. Biol.* **1992**, *227*, 1192–1204.

(39) Brünger, A. T.; Kuriyan, J.; Karplus, M. *Science* **1987**, *235*, 458–460.

(40) Nicholls, A.; Sharp, K. A.; Honig, B. *Proteins: Struct., Funct., Genet.* **1991**, *11*, 281–296.

(41) Doraiswamy, S.; Charma, D. D. *Pramana* **1974**, *2*, 219–225.

(42) Hernández-Trujillo, J.; Vela, A. *J. Phys. Chem.* **1996**, *100*, 6524–6530.